ADVANCED MATERIALS INTERFACES
www.advmatinterfaces.de

Monitoring of Dynamic Processes during Detection of Cardiac Biomarkers Using Silicon Nanowire Field-Effect Transistors

*Jie Li, Yurii Kutovyi, Ihor Zadorozhnyi, Nazarii Boichuk, and Svetlana Vitusevich**

Numerous sensitive nanobiosensors are reported for various bioassay applications as a result of the development of materials science and nanotechnology. Among these sensors, nanowire (NW) field-effect transistors (FETs) represent one of the most promising practical biosensors for ultrasensitive clinical diagnostic tools. Most studies mainly focus on how to achieve a lower detection limit but pay less attention to the long settling time effect for the detection of very small concentrations of molecules in a solution. In this study, single silicon NW FETs with long-term stability is fabricated to investigate the settling time process at small concentrations of cardiac biomarkers relevant to myocardial diseases. It is found that the settling time strongly depends on the type of molecule, its charge state and analyte concentrations. For low concentrations, the time for measurement signals to settle down is relatively long. Therefore, it is essential to understand the settling time effect in Si NW FET-based biosensing processes to ensure the accuracy and reliability of the detection signal. An alternative approach is demonstrated to circumvent the long measurement time by utilizing reaction kinetics parameters for the fast determination of low-concentration detection, which also benefits the optimal balance between suitable detection time and reliable detection results.

1. Introduction

A variety of nanomaterials and nanotechnologies have emerged in recent decades. Besides the study of novel physical properties, the main research direction is to exploit the advantages of new nanotechnologies and materials in diversified sensing applications, such as pH sensing,[1] ion sensing,[2,3] ultrasensitive detection,[4–8] precision medicine,[9,10] genetic diagnosis,[11,12] and gene sequencing.[13] As 1D nanowire structures possess a high surface/volume ratio, nanowire-based sensors demonstrate improved binding capacity and enhanced sensitivity in comparison to planar-geometry biosensors.[14] Among all the kinds of nanowire-based biosensors, silicon nanowire field-effect transistors (Si NW FETs) are promising candidates for practical early-diagnosis applications in clinical testing due to their high sensitivity and the industrially applicable complementary metal-oxide semiconductor (CMOS) fabrication process, which also permits low-cost scale-up mass manufacturing. Based on the common field-effect amplification mechanism, Si NW FETs can be a universal platform for all kinds of specific sensing purposes by various kinds of designed functionalization strategies.

Human C-reactive protein (CRP) is an acute-phase serum protein that plays a role in host innate defense. The CRP level in human blood can increase 1000-fold within 24–48 h in response to infection or inflammation.[15,16] Cardiac troponin I (cTnI) is a good biomarker of cardiovascular diseases. It has been shown that high levels of CRP together with a sudden increase of the cTnI level in the blood is closely associated with an increased risk of cardiovascular diseases.[17] For a practical biosensor, the detection limit might not be the most critical preset indicator, but stability, repeatability, and signal accuracy should be assigned more important roles, especially for biosensors for clinical or diagnostic applications. Although the detection limit of Si NW FET biosensors has reached a very low level due to competing research in order to improve sensitivity,[18–20] few researchers have mentioned the balance of sensitivity and detection time problem, especially for low-concentration detection. Usually, in the lab a CRP or cTnI test process is completed in a few minutes when samples flow through the nanodevice. However, the detection is a dynamical process and our measurements show that it requires tens of minutes or even hours for the *I–V* signal with the same sample to settle down. Underestimating the settling time (the average time required for the response curve to reach almost steady state) for detection in the test process may lead to less stringent results, and this situation becomes more critical as the very slow analyte transport process represents a detection limitation for low-concentration samples.[21] According to the biochemical reaction kinetics, the surface binding rate is very fast for high-concentration targets and it is easy to achieve a stable electrical signal in a short period of time. However, for ultralow-concentration targets,

Dr. J. Li, Y. Kutovyi, Dr. I. Zadorozhnyi, N. Boichuk, Prof. S. Vitusevich
Bioelectronics (IBI-3)
Forschungszentrum Jülich
Jülich 52425, Germany
E-mail: s.vitusevich@fz-juelich.de

The ORCID identification number(s) for the author(s) of this article can be found under https://doi.org/10.1002/admi.202000508.

DOI: 10.1002/admi.202000508

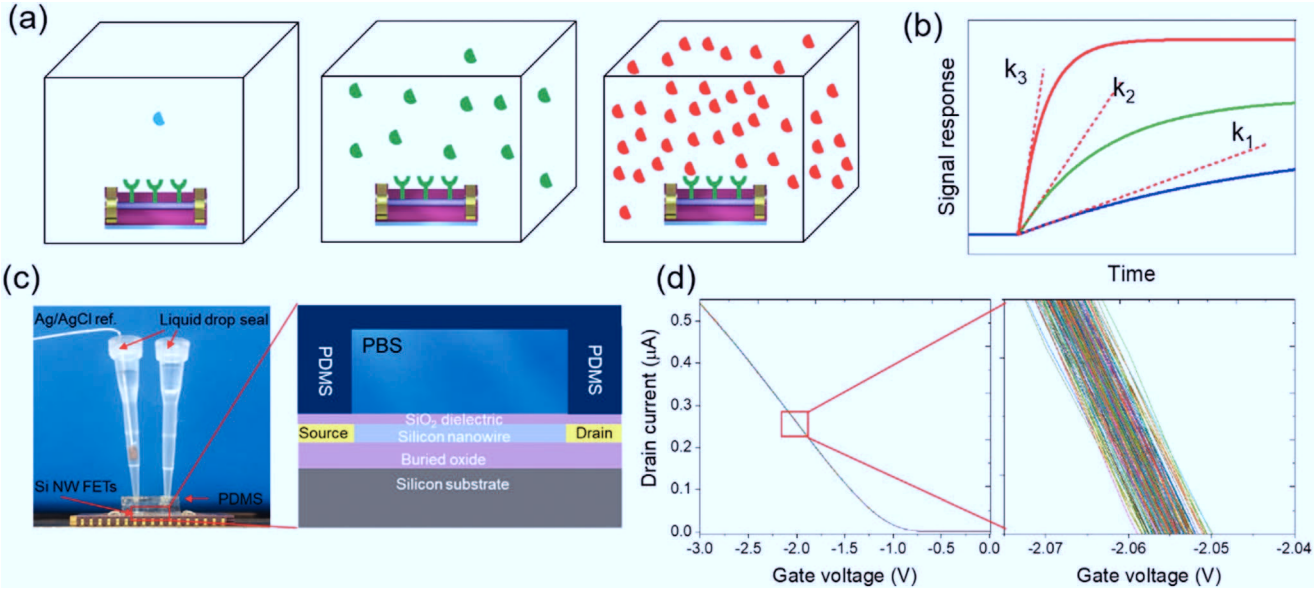

Figure 1. Schematic of settling time and concentration relationship studies for NW FET biosensors. a) Si NW FET, shown in rectangular boxes: 1, 2, and 3 under low, medium, and high concentrations of molecules in a solution, respectively; b) detection of signal response versus time under different concentrations, and different colors of the curves correspond to different concentrations in (a): k_1, k_2, and k_3 are the initial reaction rates for different concentrations (see boxes: 1, 2, and 3 of (a)) at the beginning of the detection process; c) electrical characterization of long-term stability of Si NW FET measurement unit, the enlarged schematic provides Si NW FET device layer structure information, and 1×10^{-2} M PBS 7.4 solution was sealed inside the PDMS microchamber, NW length = 4 μm, and width = 200 nm; d) long-term measurements of *I–V* characteristics for a bare chip repeated 200 times, and the enlarged part of *I–V* shows the small deviation during repeated measurements of *I–V* characteristics at V_{ds} = 0.1 V.

the corresponding settling time is greatly extended (**Figure 1**a,b). Therefore, the detection time has to be optimized for detection of low concentrations.

In this work, we studied long-time dynamic processes in Si NW FET biosensors detecting low-concentration human CRP and cTnI biomarkers. Our results show that settling time depends on the charge state of the CRP biomarker. In the case of a positive charge in pH = 7.4, this time is half as long compared to the time required for the recognition process of negatively charged CRP molecules in pH = 8.4. Also, characteristic times of the CRP kinetic process for the n-type channel and p-type channel of Si NW FET biosensors are about the same. For cTnI biomarkers, relatively long settling times were recorded for the same concentrations of molecules in the buffer solution as for the CRP biomarkers. However, this time is strongly dependent on the concentration of molecules and the response time decreases when increasing amounts of cTnI antigens are introduced into the solution. Moreover, strong changes of kinetic parameters were registered within the short time of several minutes at the beginning of the detection process demonstrating possibilities of short detection times, which are especially important in the case of strong increases in concentrations of cardiac biomarkers in the case of acute myocardial infarction.

2. Theoretical Modeling

Settling time defines the average time for a sensor output to reach and retain, within a given error band, a response signal to a given molecular input stimulus. A detectable signal change requires a sufficient number of molecules bound to the sensing region of a device. For high concentrations of biomolecules, a relatively short settling time is required. At the same time, for low concentrations of biomolecules the binding probability may be significantly reduced or the interaction time between the analytes and the surface molecular probes may be greatly increased (possibly hours or days).[22] Thus a much longer settling time is required for lower concentration detection compared to higher concentration samples.

A theoretical model has been reported for the qualitative analysis of the relationship between settling time and concentration on two types of sensor geometry: 1D nanowire sensors and 2D planar sensors.[23] As electrical signal intensity is proportional to the amount of charged molecules bound to the sensor surface, the Si NW FET surface potential change is $\Delta\varepsilon \propto N(t) \times \Delta q$. Here, $N(t)$ is the binding number of target molecules and Δq is the effective charge of the target molecule. It should be noted that $N(t)$ is a function of target density (concentration) in a given time t (diffusion effect included), see Equation below.[24,25]

Binding number of molecules on 1D nanowire sensors

$$N(t) \cong \rho_0 \times (Dt) \tag{1}$$

$$t_m \sim \frac{N_s}{D}\frac{1}{\rho_0} \tag{2}$$

Binding number of molecules on 2D planar sensors:

$$N(t) \cong \rho_0 \sqrt{(Dt)} \tag{3}$$

$$t_m \sim \frac{N_s^2}{D}\frac{1}{\rho_0^2} \tag{4}$$

where ρ_0 is the primary density of the target molecules, D is the diffusion coefficient of the target molecules, N_s is the minimum number of binding analytes to activate the sensor, and t_m is the time for the number of N_s target molecules to bind to the sensor surface. It should be noted that the diffusion coefficient of target molecules may depend on several factors, such as ion composition, ionic strength of a solution, its viscosity, and pH value.[26,27] The CRP or cTnI protein molecular weights are ≈20 kDa, diffusion coefficient D is smaller than 1 $\mu m^2\ s^{-1}$.[28] As Si NW FETs are fabricated by the top-down method on the planar wafer surface, the geometric fractal of Si NW sensors is between 1D and 2D. Note that this model attempts to qualitatively estimate the settling time scale of lower concentration detection, by calculating a 1×10^{-9} M CRP concentration sample with Equations (2) and (4), and settling time ranges between tens of seconds and several thousand seconds. As will be shown below, our experimental settling time for 4×10^{-9} M (1 μg mL^{-1}) CRP is around the 1500 s scale, which is comparable with the model prediction. In the model, we idealized that every target molecule which diffuses and collides to the surface is effective and can be captured (very sticky surface). In fact, the antibody and antigen recognition process requires many trials to match the binding site so that the true settling time might be longer than the calculated results.

3. Experimental Results and Discussion

3.1. Si NW FET Stability

Fabrication processes of the Si NW biosensors can be found in the supporting information and in previous reports.[29] Here, we fabricated SiO_2 passivated Si NW FETs of different sizes to study the biosensors' long-term stability in the phosphate buffered saline (PBS) solution. Typical sizes of the FET samples under study were as follows: nanowire field-effect transistors 4 μm in length and 200 nm in width, also relatively large-area 10 μm in length and 5 μm in width FETs were used. A special polydimethylsiloxan (PDMS) microchamber was designed and fabricated to retain the liquid for a long time (Figure 1c) by sealing the inlet and outlet with a suspended liquid drop to prevent solution evaporation. By mounting the chip on the homemade measuring set-up, the PDMS microchamber was filled with 1×10^{-2} M PBS 7.4 solution. Transfer (I–V) characteristics of the Si NW FET were measured 200 times with a constant 100 mV drain–source voltage (V_{ds}). It should be noted that the deviation of the threshold voltage or gate voltage (V_{th}) is less than 10 mV (Figure 1d).

Excellent stability and reproducible I–V characteristics were registered thus ensuring accurate and quantitative measurements in the further biosensing process. The long-term stability of the 3-aminopropyltriethoxysilan (APTES)-modified chip was also verified (**Figure 2**a), and only a small V_{th} shift was observed during measurement for 3 h. The results show that the good stability remains after silanization treatment.

3.2. Monitoring CRP Detection Process

After APTES silanization, a glutaraldehyde bifunctional bridge molecule was used to link the CRP antibody with the salinized amino group of the SiO_2 dielectric layer covering the Si NW surface. This is a common antibody modification strategy, and most reports merely give a certain antibody incubation time according to bulk reaction conditions.[30] However, the surface-interface biochemical reaction is quite different from the bulk solution reaction.[31] Here we measured the real-time shift of the I–V characteristics of Si NW chips to track the completion of surface immobilization of CRP antibodies on the nanowire surface process. After fully washing out the glutaraldehyde solution from the PDMS microchamber, a 1 μg mL^{-1} CRP antibody solution was introduced into the chamber. Then a 3 h real-time I–V was measured during this modification process (Figure 2b). At the beginning, I–V characteristic (t = 0) displayed higher conductance compared to APTES-stabilized I–V curves, due to glutaraldehyde treatment, which introduced more negative charge to the Si NW surface. With respect to the extracted V_{th} at constant drain current, a much more noticeable shift was observed compared to the bare chip and the APTES-modified chip. The extracted V_{th} shifted during the CRP antibody modification process. As can be seen from Figure 2e, it takes almost 1 h for the I–V curve to achieve the equilibrium state. This can be used as the indicator time for future antibody modification at room temperature at this concentration.

To further confirm that the number of antibodies on the silicon nanowire surface increases with extended modification time, a quantitative atomic force microscopy (AFM) characterization experiment was performed to track the density change of the surface protein particles as a function of time by dropping CRP antibody solution onto the chip surface and incubating it for a time in the range from 1 to 3 h.

As shown in Figure 2g, at the beginning the salinized chip surface was clean and flat. The number of particles on the chip surface increased with the extension of the modification time. Figure 2h shows a quantitative relationship between CRP antibody surface modification density and modification time. Except for a few large particle sizes (possibly from antibody self-cross-linking or agglomeration), most particles were of uniform size. Inset under Figure 2g shows the high-density packing, obtained after 3 h modification process, of the CRP antibody protein with a smooth surface varying in height between 2 and 3 nm. This is consistent with the characteristic size of high-density CRP antibodies on the surface.[32,33]

After the modification process with CRP antibodies, a 50% ethanolamine solution was injected into the PDMS chamber to block the unreacted aldehyde site of glutaraldehyde for 30 min. After that, the chamber was thoroughly washed with PBS to remove the excess ethanolamine, as well as unreacted absorbed antibodies. Next, 1 μg mL^{-1} of CRP antigen solution was introduced into the chamber, followed by the measurements of the I–V characteristics to study the bonding events between antibodies and CRP antigens (Figure 2c), by using the shift of the I–V characteristics. It should be noted that such a concentration of CRP solutions corresponds to a low risk of cardiac disease.[34] The extracted V_{th} at fixed drain currents displays exponential behavior. The settling time of the binding process was estimated using exponential fittings of the V_{th} shift data. The exponential decay can be described in terms of mean lifetime, τ: $V_{th} = V_{th0}\, e^{-t/\tau} + \text{const}$. Mean lifetime, or settling time, is the time at which V_{th} is reduced to 1/e ≈ 0.368 times its initial value. We repeated time-dependent measurements of CRP

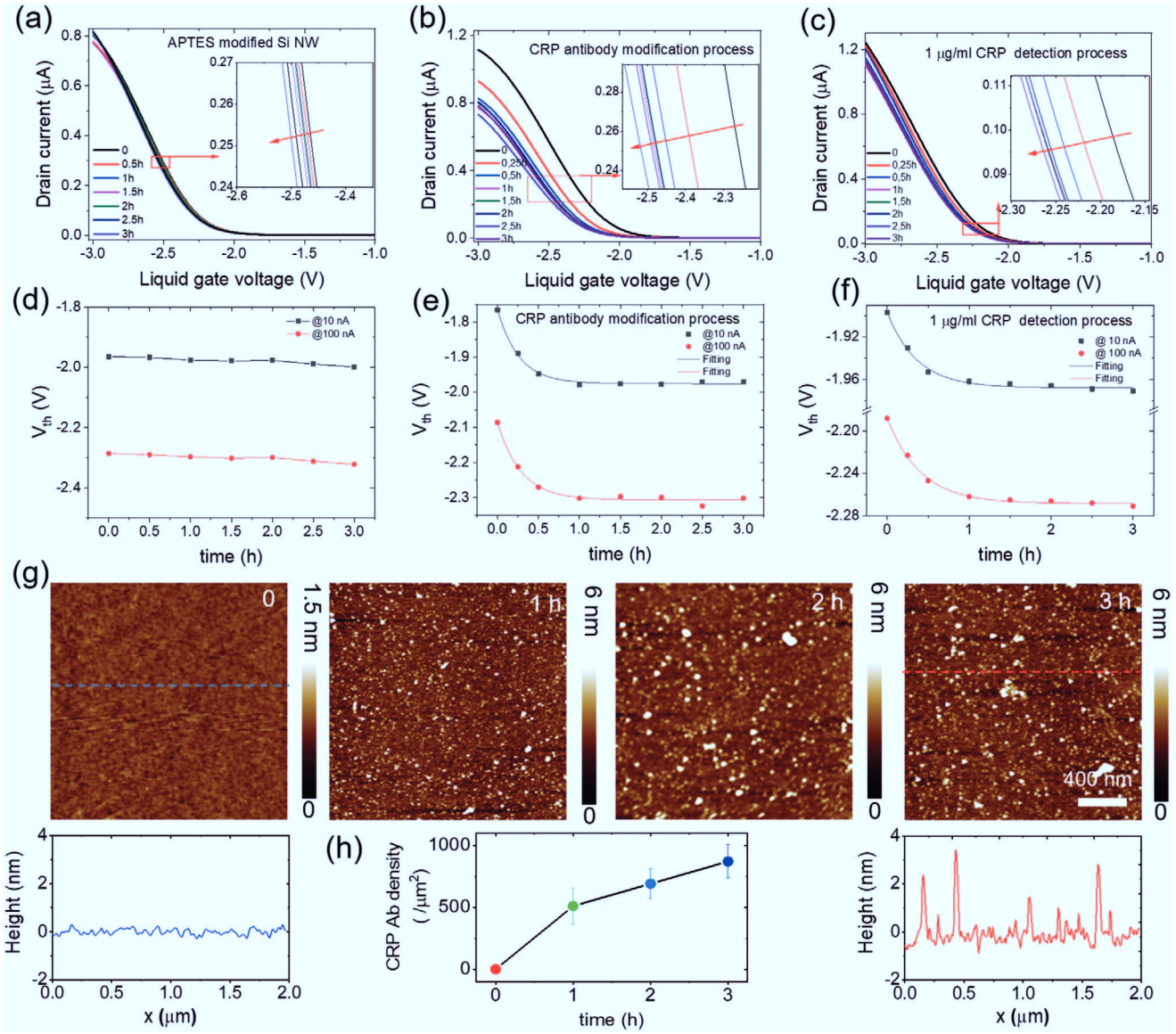

Figure 2. Long-term measurements of *I–V* characteristic shift of Si NW FETs in 1×10^{-2} M PBS solutions with pH = 7.4 during different stages: a) after APTES modification; b) during 1 μg mL^{-1} CRP antibody modification process; c) during 1 μg mL^{-1} CRP antigen detection process; inner figures are zoomed in part; (d)–(f) are extracted gate voltage at constant current 10 nA (black squares) and 100 nA (red dots), and solid curves in (e) and (f) are exponential fittings for each data set from (b) and (c), respectively; g) AFM characterization of 1 μg mL^{-1} CRP antibody modification process with different times, from 0 to 3 h with an interval of 1 h, and insets under 0 and 3 h are sections of cut lines showing the roughness of the APTES-modified substrate surface and CRP-antibody-modified surface, respectively; h) plot of CRP antibody surface density as a function of modification time from (g) with error bars.

antibody and CRP antigen processes using five different chips and found, that the average value of settling time (see **Table 1**) of CRP antigen is longer compared to the characteristic time of the CRP antibody modification process.

This fact indicates that the antigen–antibody surface reaction rate is slower than the antibody modification process compared to the antibody reaction with the aldehyde group. The antibody–antigen recognition and recombination reaction has less effective binding efficiency because it requires a higher configuration orientation match and a longer settling time for the antigen detection process compared to the antibody reaction with the aldehyde groups.

To check the selectivity and anti-interference sensing property of NW FET modified with the CRP antibodies, 10 μg mL^{-1} cTnI high concentration solution was used to study the response of the CRP antibody modified NW chip for a 3 h long-term monitoring period (**Figure 3**a). The *I–V* characteristics demonstrate a good stability (Figure 3c) while replaced with a 1 μg mL^{-1} CRP antigen + 10 μg mL^{-1} cTnI antigen mixed solution (Figure 3b). The *I–V* shift in more negative direction versus the previous experiments is registered, and the settling time extracted from the plot of V_{th} with time is 0.36 h at 10 nA and 0.37 h at 100 nA (Figure 3d), which is similar to the result obtained for 1 μg mL^{-1} CRP antigen without cTnI interference (Table 1). This proved that the NW chips

Table 1. Settling time measured after 1 μg mL^{-1} CRP antibody modification and CRP antigen detection process.

Protein[a)]		CRP antibody		CRP antigen		
Working current		At 10 nA	At 100 nA	At 10 nA	At 100 nA	At 700 nA
Settling time (h)	p-type	0.26 ± 0.02	0.29 ± 0.03	0.37 ± 0.04	0.40 ± 0.03	0.44 ± 0.03
				0.68 ± 0.06 (pH 8.4)	0.73 ± 0.05 (pH 8.4)	0.62 ± 0.02 (pH 8.4)
				0.36 ± 0.05 (+cTnI)	0.37 ± 0.05 (+cTnI)	0.44 ± 0.03 (+cTnI)
	n-type	0.27 ± 0.02	0.23 ± 0.02	0.55 ± 0.02 (from I_{ds} = 700 nA)		

[a)]All results were obtained in 1 × 10^{-2} M PBS solutions with pH 7.4, except those with a special note (pH = 8.4).

sensing selectivity has originated from the antigen–antibody specific recognition ability. Therefore, the antibody immobilized Si NW FET biosensors have demonstrated good selectivity and anti-interference properties in the complex fluid environment.

As pH is always an important factor in biochemical reactions, it may affect the biomolecule reaction rate and binding affinity and may change the charging state of the proteins. Our results show that more CRP antigens accumulating onto the Si NW surface is equivalent to an increased positive gate voltage applied to the p-type Si NW sensors, thus causing the *I*–*V* shift to a more negative direction. Here, we changed the PBS pH 7.4 to 8.4 and measured the *I*–*V* shifts of the 1 μg mL^{-1} CRP antigen process (**Figure 4**a). The shift of *I*–*V* characteristics is registered as being in the opposite direction with time, indicating that higher pH results in a changing of the charge of CRP antigens from positive to negative. This is reasonable taking into account the fact that the pH value is higher than the isoelectric point (pI) of CRP antigens (7.4).[30,35] Although the solution was prepared with the same ionic strength for the same concentration of CRP antigens, the settling time registered is almost twice the time for pH = 7.4 (Table 1), indicating that molecules in pH = 8.4 have not only the opposite charge, but also have a longer recognition time due to a reduced affinity of CRP antigen–antibody reaction. The settling time obtained from exponential fitting at 10 nA is about 0.37 and 0.68 h in solution with pH = 7.4 and pH = 8.4, respectively. It should be noted that the settling time obtained for high current at 700 nA is about the same as for low current values, i.e., is about 0.40 and 0.62 h for pH = 7.4 and pH = 8.4, respectively. All CRP antibody and antigen process settling times are summarized in Table 1.

Generally, p-type and n-type Si NW FET devices have symmetrical electrical response characteristics to bind the charged molecules: increased current in the p-type and

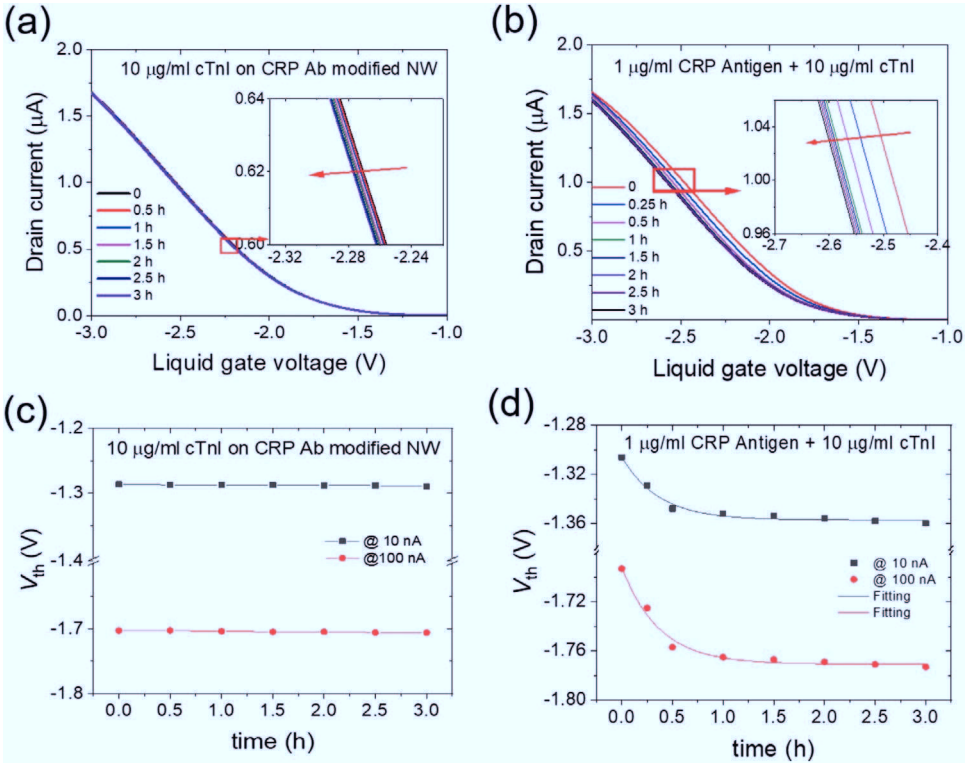

Figure 3. Demonstration of selectivity and anti-interference property of NW FET biosensors by long-term measurements of *I*–*V* characteristic shift of Si NW FETs modified with CRP antibodies: a) there is no response to 10 μg mL^{-1} cTnI antigen incubation for 3 h; b) response is registered only to CRP antigen molecules in solution composed of two mixed components: 1 μg mL^{-1} CRP antigens plus 10 μg mL^{-1} cTnI antigens; inset shows zoomed part, and arrow shows the direction of shift; (c) and (d) show extracted gate voltages at constant current 10 nA (black squares) and 100 nA (red dots) from (a) and (b); solid curves in (d) are the exponential fittings to determine the settling times.

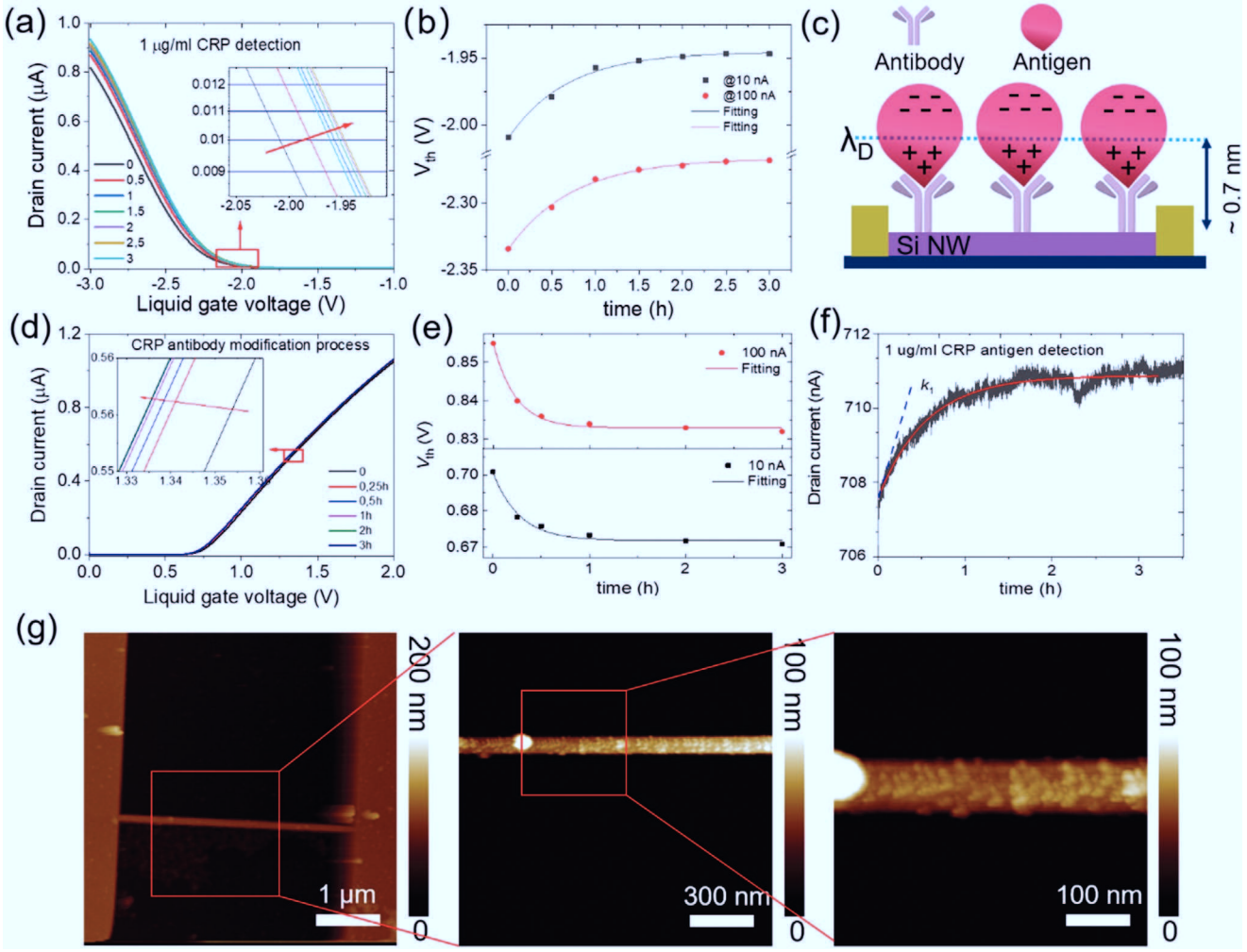

Figure 4. a) *I–V* characteristics of p-type Si NW FETs measured during 1 μg mL^{-1} CRP antigen detection process in 1×10^{-2} M PBS pH 8.4; inset in (a) shows zoomed part of V_{th} shift with time; b) extracted gate voltage at a constant current of 10 nA (black squares) and of 100 nA (red dots) from (a); c) schematic of closest binding site charge dominating the gating effect on the NW surface; d) *I–V* characteristics of n-type Si NW FETs measured in 10×10^{-3} M PBS solutions with pH = 7.4 during CRP antibody bonding process; inset to (d) shows zoomed part of shift of *I–V* characteristics to low voltage range with time; e) extracted gate voltage at a constant current of 10 nA (black squares) and of 100 nA (red dots) from (d), and red solid line is exponential fitting; f) time trace of 1 μg mL^{-1} CRP antigen detection process, $V_{ds} = 0.1$ V, $V_{lg} = 1.5$ V, red solid line is exponential fitting of time trace, and blue dashed line shows the binding rate (k_1) of 1 μg mL^{-1} CRP antigen to antibody at the very beginning of the binding process; g) AFM characterization of CRP biomarkers on NW (200 nm width and 4 μm length) after long-time detection with zoomed part to show the CRP protein complex on silicon nanowire surface.

decreased current in the n-type FET, or vice versa, depending on molecular charge state: positive or negative.

The results discussed above were obtained by studies of p-type Si NW FET chips. To confirm the results, the same modification and detection processes were also applied to n-type Si NW chips with arsenic dopants. Figure 4d shows relatively long-time measurements of *I–V* characteristic of the CRP antibody modification process on n-type chips in a solution with pH = 7.4. The V_{th} shift range is narrower and the V_{th} shifts in a lower gate voltage direction. This opposite shifting compared to the case of p-type Si NW FETs allows us to confirm that the CRP antibodies are positively charged under pH 7.4 PBS buffer, which is consistent with previous results. The settling time of the CRP antibody modification process was found to be about the same for p-type and n-type Si NW chips (Table 1). This confirms the reproducibility of the detection results.

With respect to CRP-antigen detection on the n-type of Si NW FET chips, a time trace of more than 3 h ($I_{ds} - t$) at fixed V_{ds} = 100 mV and V_{lg} = 1.5 V was measured (Figure 4f). The time trace shows exponential behavior of the drain current (I_{ds}). The average settling time for the 1 μg mL^{-1} CRP antibody modification and CRP antigen measurement process is summarized in Table 1. A relatively long settling time in the n-type Si NW FET biosensor during detection of CRP once again proved that a detectable signal change from the Si NW FET biosensor requires sufficient detection time to accumulate enough target molecules on the nanowire surface. All results were obtained in 1×10^{-2} M PBS solutions with pH = 7.4 except those with a special note (pH 8.4).

After detection of CRP biomarkers in 1 μg mL^{-1} solution for 3 h using the Si NW FET chip, the concentration of molecules was characterized by AFM. As can be seen from Figure 4g, CRP

antibody–antigen complex particles were confirmed on the Si NW surface. To estimate the CRP particles density, several regions on NW surface have been investigated using high resolution AFM. The data allow to determine the average number of CRP antigen particles, which is estimated to be ≈10 particles in 100×100 nm^2 or CRP density around 1000 μm^{-2}.

3.3. Monitoring cTnI Surface Binding Kinetics with Different Concentrations

As CRP biomarkers are predictable, but are not specific for cardiovascular damage, the cTnI biomarkers are accepted as a gold standard required to establish the diagnostic process to prevent the risk of serious sudden cardiovascular diseases. cTnI is a common cardiovascular disease marker protein and elevated levels of cTnI are directly associated with heart diseases.[36,37] Here we used the cTnI antibody-modified Si NW FETs sensors to detect cTnI. Before electrical measurement of cTnI antigens, a real-time in situ liquid AFM characterization of the cTnI antibody modification process experiment was performed. After treatment by APTES silanization and glutaraldehyde reaction, a 10 μg mL^{-1} cTnI antibody solution was injected into the AFM fluid cell on the chip surface. **Figure 5**g shows the whole AFM characterization of the cTnI antibody modification process. At the beginning, after a short time, the chip surface has only a

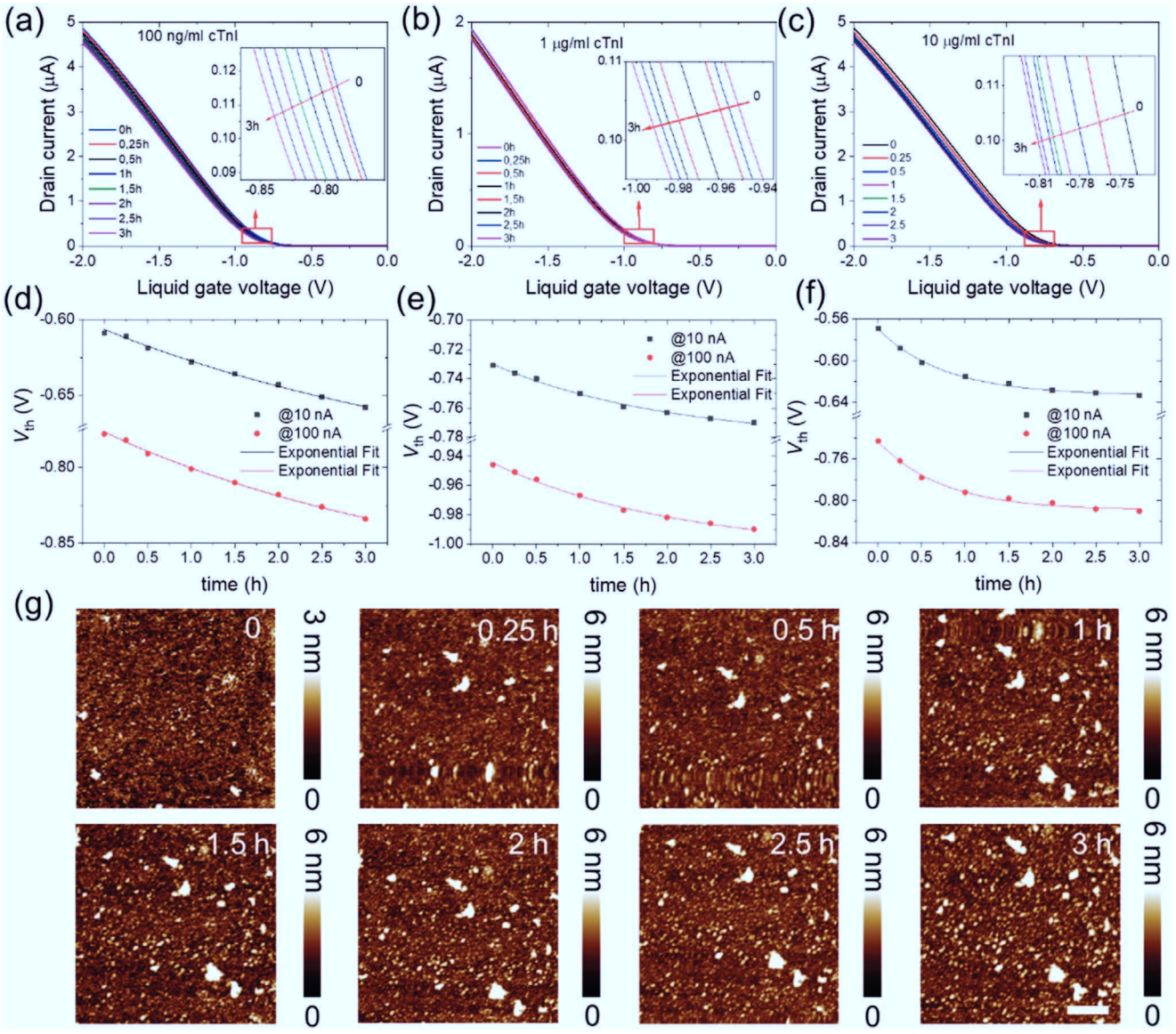

Figure 5. Long-term *I–V* characteristics of p-type Si NW FET biosensor measured in solutions with pH = 7.4 during detection process of cTnI antigen biomarkers with different concentrations: a) 100 ng mL^{-1}, b) 1 μg mL^{-1}, and c) 10 μg mL^{-1}, respectively; and insets show zoomed parts of shift (red arrow) in the *I–V* characteristics with time; (d)–(f) are corresponding extracted gate voltages from (a)–(c) at a constant current of 10 nA (black squares) and of 100 nA (red squares) with exponential fitting curves (solid lines) for each data set; g) in situ AFM characterization of 10 μg mL^{-1} cTnI solution modification process with different incubation times corresponding to measurement process of (c); scale bar: 200 nm.

few adsorbed protein particles. With increasing incubation time, more and more uniform proteins attached to the surface. After about 1 h most of the surface was covered by proteins. The estimated density of the cTnI biomarkers from the AFM image is about 2000 μm^{-2}. Then the adsorption rate and the V_{th} shift of the *I–V* characteristics slows down when the antibody modification or antigen detection process is close to the saturation stage. The AFM method allows estimating the qualitative results of antibody adsorption on NW surface to increase with time. This characterization reveals that the antibody modification process for this concentration at 10 μg mL^{-1} takes no less than 1 h.

For further experiments we used cTnI antibody-modified p-type Si NW chips to detect three different concentrations of cTnI in the range from 100 ng mL^{-1} to 10 μg mL^{-1}. The relatively long-time cTnI detection process shows that cTnI adsorption induces the *I–V* shift to a more negative direction (Figure 5a–c). The theoretical pI of cTnI is 9.87 as predicted from its amino acid sequence,[38] while the experimental results of cTnI pI determine a large discrepancy range (between pI 5.4 and 8).[39] Structural calculations also predict that the cTnI binding site is a positively charged amino-acid rich region,[40] as the cTnI size is larger than the Debye length (λ_D = 0.7 nm for 10×10^{-3} M PBS solution), and the closest binding site will dominate the gating effect of the Si NW channel (Figure 4c).

Thus, *I–V* characteristic studies of cTnI biomarkers on p-type devices show a positive charge accumulation response (V_{th} shifts to the negative voltage direction). The three V_{th}–time curves show that the signal response rates are dependent on cTnI antigen concentrations. At a 100 ng mL^{-1} concentration, the V_{th} shows a weak exponential response with a long settling time (more than 4 h), indicating a small deviation from the equilibrium state with a very slow surface binding rate compared to previous CRP detection processes. As the cTnI concentration increases to 1 μg mL^{-1}, the exponential decay behavior of V_{th}–time curve gradually enhanced with relatively shorter settling time (≈2 h). The settling time is further shortened when cTnI concentration increases to 10 μg mL^{-1} (≈0.75 h). Settling times under different cTnI antigen concentrations are summarized in **Table 2**. With the increase of the cTnI antigen concentration, the settling time significantly decreases, but it is still relatively long, even at a high concentration of 10 μg mL^{-1}. It should be noted that results obtained using different transistors as well as different chips confirm reliability of obtained data. Figure S6 in Supporting Information shows results for 10 μg mL^{-1} cTnI solution with utilization of the same method, i.e., we measured the longtime *I–V* shift, and extracted the V_{th} at 10 and 100 nA working currents. For this chip, the settling time is obtained to be 0.64 and 0.63 h at 10 and 100 nA, respectively. For the same concentration of cTnI solution for three transistors of the first chip we obtained that settling time is 0.75 and 0.71 h, respectively. The relative errors are 14.7% and 11.2%, respectively. These values are within acceptable error range taking into account 10 μg mL^{-1} low concentration of cTnI under study.

Table 2. Settling time and V_{th} response rate during detection of definite concentration of cTnI biomarkers for several concentrations: 100 ng mL^{-1}, 1 μg mL^{-1}, and 10 μg mL^{-1} in pH 7.4 PBS solutions of cTnI antigen biomarkers.

cTnI antigen concentration		100 ng mL^{-1}	1 μg mL^{-1}	10 μg mL^{-1}
Settling time [h]	At 10 nA	4.66 ± 1.63	2.04 ± 0.32	0.75 ± 0.07
	At 100 nA	4.16 ± 1.27	2.13 ± 0.34	0.71 ± 0.11
V_{th} response rate [mV h^{-1}] (initially 0.1 h)	At 100 nA	18.67	27.02	76.61

cTnI fast detection is very demanding for the analysis of major adverse cardiovascular events, such as acute myocardial disease. In most cases, the detection readout of FET-based biosensors is based on the change of direct measurement parameters such as current, conductance and voltage. With respect to ultralow concentration detection with nanoscale biosensors, a long response time could be one of the major obstacles for nanobiosensor applications.

In order to obtain a reliable readable signal in a practical measurement time, one possibility is to use kinetic parameters to acquire target concentration information. For this purpose, the antibody–antigen binding reaction can be described as Equation (5). In the equation, "*A*" represents the quantity of target molecules (antigens), "*B*" represents the quantity of probe molecules (antibodies), and "*AB*" stands for reaction products. As the NW surface potential change is proportional to the number of targets attached to the NW surface, the reaction equation rate follows Equation (6).

3.4. Monitoring of Binding Kinetic of Molecules Using Kinetic Model

Considering that at the beginning the antigen–antibody complex density [*AB*] is equal to 0, Equation (6) approximately results in Equation (7), which represents the rate of surface potential change starting at the moment $t = 0$. Its value is proportional to the initial bulk concentration of antigens, which is the object of interest. Therefore, by fitting the V_{th} shift with time curve using the kinetic model, it is possible to obtain the binding reaction rate value which includes information about the target concentration (Figure 1b).

$$A + B \rightleftharpoons AB \tag{5}$$

$$\frac{dV_{th}}{dt} \sim \frac{d[AB]}{dt} = k_a [A]_0 \left([B]_0 - [AB]\right) - k_d [AB] \tag{6}$$

$$\left.\frac{dV_{th}}{dt}\right|_{t=0} \cong k_a [A]_0 [B]_0 \tag{7}$$

where k_a is the association rate constant, k_d is the dissociation rate constant, and $[A]_0$ and $[B]_0$ represent the initial bulk and surface concentrations, respectively. It should be noted that response rate can be determined within 0.1 h (see detailed explanation in the Supporting Information) taking into account characteristic settling times, obtained in our experiment.

Here we measured response of NW FET sensors to the cTnI in the concentration range from 100 ng mL^{-1} to 10 μg mL^{-1} and plotted V_{th}–time curve to obtain the relationship of the V_{th} response rate versus concentration. **Figure 6** shows the plots of

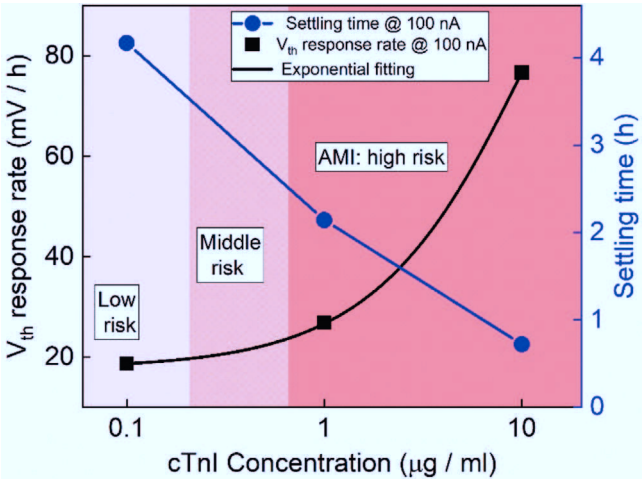

Figure 6. V_{th} response rate and settling time versus cTnI antigen concentrations, and different concentration ranges marked with colors to show the relationship of myocardial damage risk probability with increase of cTnI concentration. Ranges demonstrate the tendency of the response rate to speed up with increasing molecular concentration. Selected ranges for biomedical diagnostics can be found in ref. [41].

V_{th} response rate taken within first 0.1 h and settling time with increase of cTnI concentrations at 100 nA current. The obtained tendency is correlated with selected ranges for biomedical diagnostics.[41] Compared to the linear decrease in settling time, the exponential increase in V_{th} response rate indicates that the initial kinetic antigen–antibody binding process is more sensitive to cTnI concentration change. The fact further proves the benefit of kinetic model for rapid detection strategy. The results reflect the fact that for ultralow cTnI sample detection it is possible to read out the concentration from the V_{th} response rate curve within a few minutes, rather than applying a longer time test. Due to the differences of biomarker concentration in different individuals, each biomarker concentration has a certain interval distribution such as the reference interval on a common medical checklist or calibration curve. Knowledge of the interval in which cTnI level is more realistic than its absolute value, so that this feature facilitates early and rapid diagnosis within about 6 min and allows analysts to initially obtain the cTnI level on a practical time scale for adequate diagnostic performance. Figure 6 schematically shows the positive correlation between cardiac disease risk and the cTnI level.

The intrinsic response of Si NW FETs is fast, but the nature of the surface acceptor-receptor recognition and binding process during detection may be slow, especially for small concentrations and low diffusion coefficients of the macrobiomolecular detection process, which is the rate-determining step. Therefore, the response time and sensitivity will be similar to the complementary variables in the Heisenberg uncertainty principle and will have a mutually restrictive relationship.

4. Conclusions

Practical sensing applications require fast and accurate detection. In this work, we studied the settling time effect on the antibody modification and antigen detection process of cardiac CRP and cTnI biomarkers. These biomarkers are often used for early diagnosis of cardiovascular diseases. Our results show that under a fixed concentration of biomarkers and a certain value of current in the nanowire channel the electrical signal (V_{th} shift) has a relatively long-time dependence, which is different from the traditional step-like electrical signal usually observed for high concentrations of molecules in solution. This relatively slow dynamic process for target cTnI biomolecules of recognition and binding on the NW surface is considerably shorter (about five times) for target CRP biomarkers. Moreover, the settling time determined for negatively charged CRP biomarkers in solution with pH = 8.4 is twice as great compared to the time estimated for positively charged CRP biomarkers in pH = 7.4. The results should be taken into account in order to optimize the time parameters of cardiac biosensors. In situ AFM characterizations visualized the accumulation binding process after NW modification with antibodies followed by bonding of antigens. An alternative strategy to read out the ultralow biomarker level in a practical time of several minutes is to utilize the kinetics parameter of the surface binding process, i.e., the signal response rate. In this method, the concentration dependence during the detection process makes it possible to acquire the information about small concentration of target biomolecules in a practical measurement time.

5. Perspectives

Recognizing that low concentration sensing requires a relatively long settling time will not compromise the practical application value of Si NW biosensors. Instead we can better understand and improve the test conditions[21,42,43] or strategies[26] to ensure the accuracy of detection results by utilizing, for example, the following methods: selecting high binding affinity receptors as recognition probes; improving biomolecular mass transport rate within the microchannel to accelerate the analyte flow rate to the Si NW FET surface; utilizing electrostatic fields allowing drift transport of biomolecules to the surface; specifically defining the sensing area exactly on NW (instead of surface functionalization of the entire chip area). The latter procedure makes it possible to suppress ineffective substrate competitive bindings of molecules and increase binding events on the nanowire. As the accuracy and reliability of detection results are important parameters in line with the detection time and low detection limit, an optimal balance between sensitivity and practical detection time has to be selected. This will promote the maturity, transformation, and application of this nanobioelectronic sensing technology.

6. Experimental Section

Si NW FET Fabrication: Details of fabrication protocols can also be found in previous reports.[29,44] The devices were fabricated with a top-down approach by a fabrication process compatible with complementary metal-oxide-semiconductors (CMOSs). Transistors were fabricated on 4 in. p-type silicon-on-insulator (SOI) wafers (SOITEC, France). The SOI wafers have a 50 nm p-type (10^{15} cm^{-3} boron-doped) ⟨100⟩ layer of active silicon and a 145 nm thick buried oxide (BOX) layer separated the active silicon layer from the highly doped silicon substrate (10^{17} cm^{-3}

boron-doped). A 20 nm thick silicon dioxide (SiO_2) layer was deposited on top by the plasma-enhanced chemical vapor deposition method. This layer was used for the wet chemical etching process as the hard mask for nanowire patterning. The small nanowire pattern was defined by e-beam lithography and large MEZA structures were defined by photolithography. Then, an anisotropic wet etching process was performed with 5% tetramethylammonium hydroxide (TMAH) at 80 °C to form the nanostructures. Next, a boron ion implantation process with an energy of 6 keV and a dose of 1×10^{15} cm^{-2} was performed to form an accumulation mode transistor structure (p^+–p–p^+). The wafers were then thermally annealed for 5 s at 1000 °C and an 8 nm thick SiO_2 layer was thermally grown on the NW surface as the dielectric layer. Then, 5 nm Cr + 200 nm Al was sputter-deposited to form metallic contact feedlines to the Si NW FETs using the lift-off process. Afterward, the metalized structures were annealed in a forming gas atmosphere for 1 min at 450 °C to form good ohmic contacts. Finally, the feedlines were passivated with a 2 µm thick polyimide layer and then the silicon nanowire sensing area was opened using photolithography. The final step was to cut the wafers into 1 cm × 1 cm chips. All the fabrication processes of Si NW FET devices were performed in the Helmholtz Nano Facility (HNF) of Forschungszentrum Jülich GmbH (FZJ).

Device Functionalization: After fabrication, the chip was glued onto a carrier with silver paste and appropriately wire-bonded to match the measurement socket. Then, we used oxygen plasma (Diener electronic plasma oven) at 0.8 mbar and 80 W for 5 min to activate and clean the nanowire surface. After activation, the chip was placed into a desiccator in a glove box with 200 µL APTES in an open plate, and the nanostructures were silanized by APTES vapor at 5 mbar pressure (argon-protected) for 1 h. After silanization, the devices were rinsed with pure ethanol several times to remove physically adsorbed APTES and dried by a N_2 gun. Annealing was next performed for 5 min at 110 °C on the hotplate. This heat dehydration process allows the bonding between the ATPES and the chip surface to be improved. The next step was to drop a bifunctional linker 2.5% glutaraldehyde (Sigma Aldrich) on the chip surface to react with the amine terminal of the nanowire surface APTES for 1 h at room temperature. All CRP and cTnI samples were purchased from Sigma-Aldrich.

Electrical Sensing Setup: Current–voltage electrical measurements were performed using Keithley 2430 and Keithley 2400 (Keithley Instruments Inc., Cleveland) source-meter units (SMUs). A Python-based software package developed in-house was used to control both the drain–source and liquid-gate SMUs. In order to avoid solution evaporation during long-time measurements, a PDMS mold with a cylindrical inner chamber (diameter $\varnothing = 3$ mm, height $H = 2$ mm, and volume $V \approx 14$ µL) was designed, fabricated, and attached to the Si NW chip. The chamber was then filled with solution and the inlet and outlet sealed with a liquid drop. A stable long-term electrical measurement unit was thus fabricated (Figure S3a, Supporting Information). All electrical measurements were performed at room temperature inside a metal Faraday cage in order to shield the device from external electromagnetic fields. A standard Ag/AgCl reference electrode was used to apply the liquid-gate voltage.

Supporting Information

Supporting Information is available from the Wiley Online Library or from the author.

Acknowledgements

The authors are grateful to the anonymous referees for their constructive criticism. Jie Li would like to acknowledge bilateral support from the 2018 Helmholtz–OCPC–Program and the Shanghai Institute of Microsystem and Information Technology (SIMIT). Yurii Kutovyi greatly appreciates a research grant from the German Academic Exchange Service (DAAD). The authors also thank all the technical staff of the Helmholtz Nano Facility (HNF) of Forschungszentrum Jülich for their assistance with fabrication of the sensor devices.

Conflict of Interest

The authors declare no conflict of interest.

Keywords

biosensors, cardiac biomarkers, field-effect transistors, settling time, silicon nanowires

Received: March 23, 2020
Revised: May 6, 2020
Published online: June 3, 2020

[1] Y. Cui, Q. Wei, H. Park, C. M. Lieber, *Science* **2001**, *293*, 1289.
[2] R. Sivakumarasamy, R. Hartkamp, B. Siboulet, J. F. Dufrêche, K. Nishiguchi, A. Fujiwara, N. Clément, *Nat. Mater.* **2018**, *17*, 464.
[3] M. Wipf, R. Stoop, A. Tarasov, K. Bedner, W. Fu, I. Wright, C. Martin, E. Constable, M. Calame, C. Schoenenberger, *ACS Nano* **2013**, *7*, 5978.
[4] F. Patolsky, G. Zheng, C. M. Lieber, *Nat. Protoc.* **2006**, *1*, 1711.
[5] S. Vitusevich, I. Zadorozhnyi, *Semicond. Sci. Technol.* **2017**, *32*, 043002.
[6] I. Zadorozhnyi, J. Li, S. Pud, H. Hlukhova, V. Handziuk, Y. Kutovyi, M. Petrychuk, S. Vitusevich, *Small* **2017**, *14*, 1702516.
[7] Y. Kutovyi, H. Hlukohova, N. Boichuk, M. Menger, A. Offenhaeusser, S. Vitusevich, *Biosens. Bioelectron.* **2020**, *154*, 112053.
[8] Y. Fu, N. Wang, A. Yang, H. Law, L. Li, F. Yan, *Adv. Mater.* **2017**, *29*, 1703787.
[9] N. C. S. Vieira, A. Figueiredo, J. F. dos Santos, S. M. Aoki, F. E. G. Guimarães, V. Zucolotto, *Anal. Methods* **2014**, *6*, 8882.
[10] G. Zheng, F. Patolsky, Y. Cui, W. U. Wang, C. M. Lieber, *Nat. Biotechnol.* **2005**, *23*, 1294.
[11] R. Etzioni, N. Urban, S. Ramsey, M. McIntosh, S. Schwartz, B. Reid, J. Radich, G. Anderson, L. Hartwell, *Nat. Rev. Cancer* **2003**, *3*, 243.
[12] G. He, J. Li, C. Qi, X. Guo, *Adv. Sci.* **2017**, *4*, 1700158.
[13] S. Howorka, Z. Siwy, *Chem. Soc. Rev.* **2009**, *38*, 2360.
[14] Y. Wang, T. Wang, P. Da, M. Xu, H. Wu, G. Zheng, *Adv. Mater.* **2013**, *25*, 5177.
[15] A. Bíró, Z. Rovó, D. Papp, L. Cervenak, L. Varga, G. Füst, N. M. Thielens, G. J. Arlaud, Z. Prohászka, *Immunology* **2007**, *121*, 40.
[16] J. Danesh, J. G. Wheeler, G. M. Hirschfield, S. Eda, G. Eiriksdottir, A. Rumley, G. D. Lowe, M. B. Pepys, V. Gudnason, *N. Engl. J. Med.* **2004**, *350*, 1387.
[17] T. Lee, J.-H. Ahn, J. Choi, Y. Lee, J.-M. Kim, C. Park, H. Jang, T.-H. Kim, M.-H. Lee, *Micromachines* **2019**, *10*, 203.
[18] J. Li, G. He, H. Ueno, C. Jia, H. Noji, C. Qi, X. Guo, *Nanoscale* **2016**, *8*, 16172.
[19] G. He, J. Li, H. Ci, C. Qi, X. Guo, *Angew. Chem., Int. Ed.* **2016**, *55*, 9036.
[20] J. Li, G. He, U. Hiroshi, W. Liu, H. Noji, C. Qi, X. Guo, *ACS Nano* **2017**, *11*, 12789.
[21] P. E. Sheehan, L. J. Whitman, *Nano Lett.* **2005**, *5*, 803.
[22] X. Duan, Y. Li, N. K. Rajan, D. A. Routenberg, Y. Modis, M. A. Reed, *Nat. Nanotechnol.* **2012**, *7*, 401.
[23] P. R. Nair, M. A. Alam, *Appl. Phys. Lett.* **2006**, *88*, 233120.
[24] A. Giridhar, P. R. Kumar, in *Proc. 4th Int. Symp. on Information Processing in Sensor Networks*, (Eds: M. Vetterli, K. Yao), IEEE Press, Los Angeles, CA **2005**, p. 2.

[25] a) J.-I. Hahm, C. M. Lieber, *Nano Lett.* **2004**, *4*, 51; b) P. Rao, *Int. J. Nanotechnol. Appl.* **2017**, *11*, 213.
[26] T. M. Squires, R. J. Messinger, S. R. Manalis, *Nat. Biotechnol.* **2008**, *26*, 417.
[27] Y.-J. Fun, H.-J. Sheen, Z.-Y Chen, Y.-H Liu, J.-F Tsai, K.-C Wu, *Microfluid. Nanofluid.* **2015**, *19*, 85.
[28] R. P. Ron Milo, *Cell Biology by the Numbers*, 1st ed., Garland Science, New York **2015**.
[29] Y. Kutovyi, I. Zadorozhnyi, H. Hlukhova, V. Handziuk, M. Petrychuk, A. Ivanchuk, S. Vitusevich, *Nanotechnology* **2018**, *29*, 175202.
[30] M. Tsujimoto, K. Inoue, S. Nojima, *J. Biochem.* **1983**, *94*, 1367.
[31] S. K. Singh, A. Thirumalai, A. Pathak, D. N. Ngwa, A. Agrawal, *J. Biol. Chem.* **2017**, *292*, 3129.
[32] R. Funari, B. Della Ventura, C. Altucci, A. Offenhausser, D. Mayer, R. Velotta, *Langmuir* **2016**, *32*, 8084.
[33] S. Lin, C.-K. Lee, Y.-M. Wang, L.-S. Huang, Y.-H. Lin, S.-Y. Lee, B.-C. Sheu, S.-M. Hsu, *Biosens. Bioelectron.* **2006**, *22*, 323.
[34] P. M. Ridker, *Circulation* **2003**, *108*, e81.
[35] F. Patolsky, G. Zheng, C. M. Lieber, *Nanomedicine* **2006**, *1*, 51.
[36] L. Babuin, A. S. Jaffe, *Can. Med. Assoc. J.* **2005**, *173*, 1191.
[37] K. Kim, C. Park, D. Kwon, D. Kim, M. Meyyappan, S. Jeon, J.-S. Lee, *Biosens. Bioelectron.* **2016**, *77*, 695.
[38] B. Bjellqvist, G. J. Hughes, C. Pasquali, N. Paquet, F. Ravier, J. C. Sanchez, S. Frutiger, D. Hochstrasser, *Electrophoresis* **1993**, *14*, 1023.
[39] E. Peronnet, L. Becquart, J. Martinez, J.-P. Charrier, C. Jolivet-Reynaud, *Clin. Chim. Acta* **2007**, *377*, 243.
[40] J. Sabek, P. Martínez-Pérez, J. García-Rupérez, in *Multidisciplinary Digital Publishing Institute Proceedings*, Vol. *4*, **2018**, p. 41.
[41] M. F. M. Fathil, M. K. Md Arshad, S. C. B. Gopinath, U. Hashim, R. Adzhri, R. M . Ayub, A. R. Ruslinda, M. Nuzaihan, A. H. Azman, M. Zaki, T.-H. Tahg, *Biosens. Bioelectron.* **2015**, *70*, 209.
[42] M. J. Heller, A. H. Forster, E. Tu, *Electrophoresis* **2000**, *21*, 157.
[43] P. Katira, H . Hess, *Nano Lett.* **2010**, *10*, 567.
[44] I. Zadorozhnyi, *Ph.D. Thesis*, Forschungszentrum Juelich and TU Dortmund University, Germany **2019**.